# Effect of Bonding Area on Bond Stress Behavior of GFRP Bars in Concrete

Fakhruddin [1, 2]*, Kusnadi [3], Rudy Djamaluddin [1], Rita Irmawaty [1],
Suharman Hamzah [1], Luna N. Ngeljaratan [2]

[1] Department of Civil Engineering, Faculty of Engineering, Universitas Hasanuddin, Makassar, 92171, Indonesia.

[2] Research Centre for Structural Strength Technology, National Research and Innovation Agency, Indonesia.

[3] Department of Civil Engineering, Faculty of Engineering, Universitas Khairun, Ternate, 97719, Indonesia.

## Abstract

The application of Glass Fiber Reinforced Polymer (GFRP) bars is suitable for concrete structures that are susceptible to corrosion, owing to their corrosion-resistant characteristics. Therefore, it is feasible to reduce the concrete cover on reinforced concrete beams by utilizing GFRP bars. However, this can reduce the bonding strength between GFRP bars and concrete. Therefore, this study aims to investigate the bonding behavior between GFRP bars and concrete as a preliminary test for structural applications. The bond stress behavior between GFRP bars and concrete was analyzed by 18 pull-out tests. The test specimens comprised GFRP bars with three different variations, namely GFRP bars with concrete cover (GFRP-C), GFRP bars without concrete cover (GFRP-E), and GFRP bars with a complete wrapping of GFRP sheet (GFRP-C-Sheet). The bond stress-slip curve, bond strength, and failure pattern were utilized to analyze the effect of each variation. The research results indicate that the bonding stress between GFRP bars and concrete was strongly influenced by the concrete cover, where the bonding strength decreased by 65%. Nevertheless, the utilization of a complete wrapping GFR) sheet resulted in a 26.4% increase in bonding stress. The present study has identified three distinct modes of failure, including pull-out (GFRP-C), concrete crushing (GFRP-E), and GFRP sheet debonding (GFRP-C-Sheet).

*Keywords:* Bond Strength; Centric Bars; Eccentric Bars; GFRP Bars; Pull Out.

## 1. Introduction

The corrosion of steel reinforcement is a prevalent issue that frequently arises in concrete structures situated in aggressive environments. The volumetric expansion of the corrosion products exceeds that of the original cross-sectional area of the reinforcement. The phenomenon of volume expansion results in an increase in the radial pressure at the interface of steel and concrete. This pressure leads to cracking along the reinforcement and spalling of the concrete cover. This damage can decrease the durability of the structure; if the appropriate repair methods are not taken, it will cause structural failure. Therefore, corrosion-resistant reinforcement is needed to replace conventional reinforcement, especially for structures in aggressive environments. The utilization of fiber-reinforced polymer (FRP) bars has been identified as a viable substitute for traditional reinforcement methods. According to literature, FRP bars exhibit several advantages over traditional steel reinforcement, including their non-corrosive and non-conductive properties, high strength-to-weight ratio, cost-effectiveness, and superior resistance to corrosion [1, 2].

FRP bars can be made from glass, carbon, aramid, and basalt. The process of creating reinforcement involves the binding of fibers through the application of epoxy resins, including but not limited to polyester, vinyl ester, and epoxy. The mechanical properties and surface shape of FRP bars are very different from those of conventional reinforcement. According to Solyom et al. [3], the tensile strength and elastic modulus of FRP bars are strongly influenced by the properties and volume of fiber used. The tensile strength of FRP bars ranges from 450-3500 MPa, while the elastic modulus ranges from 35-580 GPa. Failure strains varied between 0.5-4.4%. In addition, FRP bars have linear elastic behavior until failure without any plasticity [3–5].

The bond stress characteristic between GFRP bars and concrete is the most critically studied parameter. In contrast to steel reinforcement, the behavior of GFRP material is characterized by anisotropy, non-homogeneity, and linearity, leading to a distinct mechanism of force transfer between the reinforcement and concrete. The bonding behavior of concrete is influenced by several primary factors [6-22], including concrete strength, concrete cover, bar diameter, surface characteristics, embedment length, and rib geometry. The bond strength of GFRP bar and concrete is also influenced by elevated temperatures [23–26]. Many studies have been done to understand the bond characteristics between FRP bars and concrete, but many aspects remain to be studied.

Corrosion-resistant properties of GFRP bars make it possible for maximal lowering of concrete cover on reinforced concrete beams. The effective height of the beam will increase so that the resulting moment capacity is greater than the reinforcement with a concrete cover. However, this will affect the load transfer between the GFRP bars and the concrete because the bonding area is reduced. Therefore, it is necessary to increase the bond strength of eccentric bars by using GFRP sheet. GFRP sheet in this study act as external shear reinforcement in RC beam applications.

The mentioned and other works show considerable research on bond behavior. However, there are still no studies related to GFRP bond behavior without concrete cover and with the addition of a full wrapping GFRP sheet. Therefore, this study aims to examine the bond stress characteristics between concrete and GFRP bars through the implementation of a pull-out test. The study focused on both centric and eccentric GFRP bars that have been embedded in the concrete. The experimental procedures were conducted in accordance with the ACI 440.3R-04 standard [27]. An eccentric pull-out test was conducted for specimens without concrete cover where the GFRP bars are positioned close to the specimen side. Other specimens were prepared with a GFRP sheet surrounding the concrete cube to increase the bonding stress between the eccentric GFRP bars and concrete. Finally, the results of this study were discussed in terms of the bonding stress-slip relationship, maximum bonding stress, and failure mode.
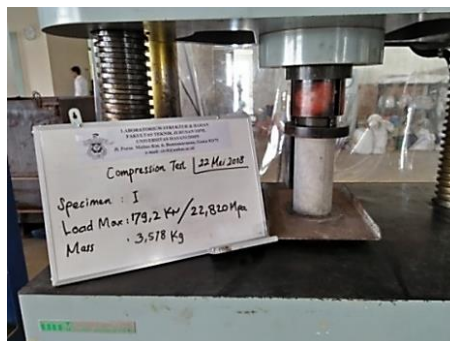
## 2. Experimental Programs

### 2.1. Concrete

The mix design of concrete is presented in Table 1. The design compressive strength of the concrete was 20 MPa and the water cement ratio (w/c) was 0.5. The concrete is mixed using a concrete pan capacity of 0.2 liters. Cylindrical sampling was carried out when casting to determine the actual concrete strength. The concrete strength test was conducted using a universal testing machine (Figure 1), and the results showed that the average compressive strength of concrete at 28 days was 24.6 MPa.

**Table 1. Mix design of concrete (kg/m$^3$)**

| Cement | Water | Sand | Gravel |
|--------|-------|------|--------|
| 180 | 370 | 523 | 1276 |



**Figure 1. Compression strength test of concrete specimens**

### 2.2. GFRP Bars and GFRP Sheets

The GFRP bar and sheet utilized in this work are shown in Figure 2. The diameter of GFRP bars was 13 mm. GFRP bars are a composite mixture of high-strength glass fiber and polyester resin, vinyl ester resin and epoxy resin. The characteristic of GFRP bars was based on the properties determined by the manufacturer, as shown in Table 2.

(a) GFRP bar                                               (b) GFRP sheet

**Figure 2. GFRP bars and sheet**

**Table 2. GFRP bar properties**

| Properties | Testing properties | Design properties |
|---|---|---|
| Nominal diameter | 12.7 mm | 12.7 mm |
| Area | 129 mm$^2$ | 129 mm$^2$ |
| Elastic modulus | 43.9 GPa | - |
| Ultimate tensile strength | 788 MPa | 708 MPa |
| Ultimate strain | 1.79 % | - |

The equivalent diameter is needed to determine the cross-section area of GFRP bars. The equivalent diameter test was conducted using ACI 440.3R-04 code [27]. The process of testing the equivalent diameter of GFRP bars was as follows: (1) Put GFRP bars for at least 24 hours before testing, (2) Fill the measuring cylinder glass with enough water or ethanol to avoid overflow to prevent water overflow when inserting GFRP bar, (3) Measure the length of the specimen three times, with each measurement rotated to 120$^o$, (4) Before inserting the specimen, measure the volume of water or ethanol in the measuring cylinder glass, then insert the GFRP bars. Ensure no water or ethanol overflows after inserting the specimen and no air is trapped. Then measure the increase in volume, (5) Calculate the cross-sectional area based on the ACI 440.3R-04 formula:

$$A = \frac{\Delta V}{L} = \frac{V_1 - V_0}{L} \times 1000 \tag{1}$$

where $\Delta V$ is the increased volume of water or ethanol, $V_0$ is the initial volume, $V_1$ is the final volume and $L$ is the length of GFRP bars. From the test results, the equivalent diameter of GFRP bar was 12.63 mm (Figure 3).



(a) Preparation of GFRP bars                                               (b) Measure the length of GFRP bars



(c) Put the GFRP bars into cylinder glass
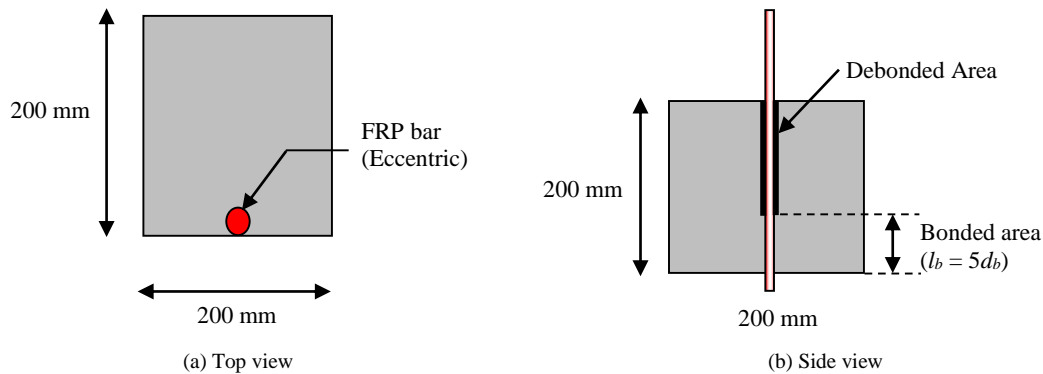
**Figure 3. Diameter equivalent test of GFRP bars**

This study also used the GFRP sheet to increase the bonding stress between GFRP bar and concrete. In the beam application, this GRFP sheet will be applied with U-shape configuration. The properties of GFRP sheet obtained from the manufacturer was shown in Table 3.

**Table 3. Composite gross GFRP laminate properties**

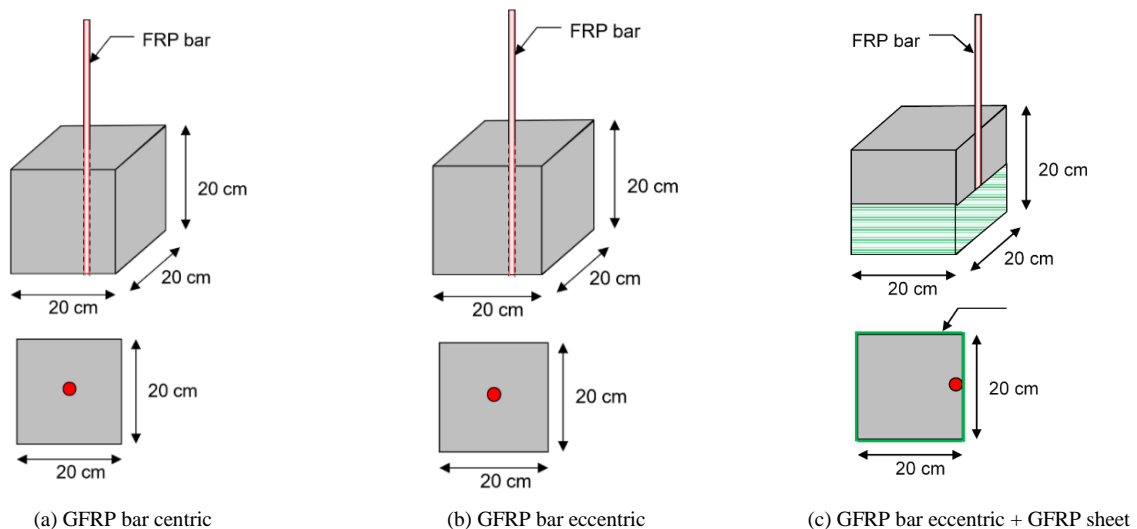| Properties | ASTM Method | ACI 440.2R properties [22] | Design properties |
|---|---|---|---|
| Ultimate tensile strength | | 575 MPa | 460 MPa |
| Elongation at break | D3039 | 2.20% | 2.20% |
| Young modulus | | 26.1 GPa | 20.9 GPa |
| Nominal laminate thickness | D1777 | 1.3 mm | 1.3 mm |

## 2.3. Pull-Out Specimens

The pull-out specimens were designed according to Veljkovic et al. [15] and ACI 440.3R-04 standard [27]. A 200 mm cubic mold was used to fabricate the specimens. Each specimen consisted of a concrete cube with a single bar embedded vertically in the center (centric specimens) and at the edge (eccentric specimens) of the cube. The bonded length of the bars was determined to be five times the diameter of the bar ($lb = 5db$) and positioned at the lowermost part of the concrete cube, as shown in Figure 4.



**Figure 4. Geometry of eccentric pull-out specimens**

A set of 18 specimens, each having a cube shape, were fabricated and subjected to a pull-out test (Table 4). During the concrete pouring process, the wooden formwork was integrated with FRP bars. The specimens were moved to the curing room for a duration of 28 days, following the casting process, and the formwork was removed a day after. The variation of specimens was the location of GFRP bars and the addition of GFRP sheet. GFRP-C is the specimens with concrete cover where the location of GFRP bars at the center cube specimens (centric). The GFRP-E was the specimens without concrete cover where the location of GFRP bars at the edge of cube specimens (eccentric). Meanwhile, GFRP-E-Sheet was specimens without concrete cover and with the addition of a full wrapping GFRP sheet. The specimen design is shown in Figure 5.
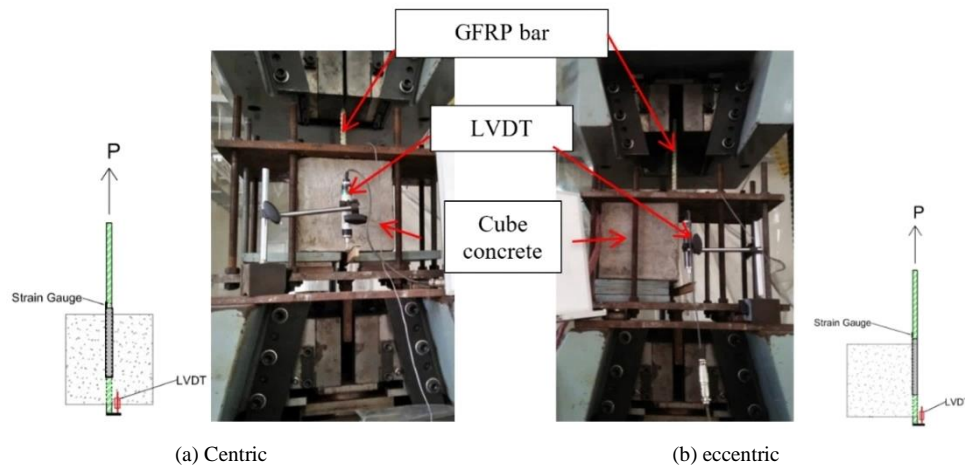


**Figure 5. The specimens design**

**Table 4. Variation of specimens**

| Specimens | Location of GFRP bars | GFRP Sheet | Number of specimens |
|---|---|---|---|
| GFRP-C | Centric (middle) | - | 6 |
| GFRP-E | Eccentric (edge) | - | 6 |
| GFRP-E-Sheet | Eccentric (edge) | Yes | 6 |

## 2.4. Loading Setup and Testing Equipment

The pull-out test setup is shown in Figure 6. The test was conducted at 28 days using a Universal Testing Machine with a capacity of 1000 kN. The displacement control was chosen for the purpose of observing the post-peak behavior of materials. The GFRP bars were subjected to a load of 0.2 mm/min and the load was measured using a load cell connected to the loading machine. During the loading test, a strain gauge was mounted at the mid-span of GFRP bars to quantify the strain. Furthermore, the installation of LVDT was carried out to acquire the slip behavior of the specimens. The digital data logger was utilized to record all of the data.



(a) Centric                                                          (b) eccentric

**Figure 6. Pull-out test**

## 3. Results and Discussion

### 3.1. Bond stress

The pull-out test aims to determine the bond stress between GFRP bars and concrete. The calculation of bond stress refers to ACI 440.3R-04 [27], as shown in Equation 2.

$$\tau = \frac{P}{\pi . d_b . l_b .}$$                                                                                                                                            (2)

where P is the tensile force (*N*), $d_b$ is the rebar diameter, and $L_b$ is the embedment length (*mm*). The experimental results obtained from the bond test and the mode of failure are presented in Table 5.
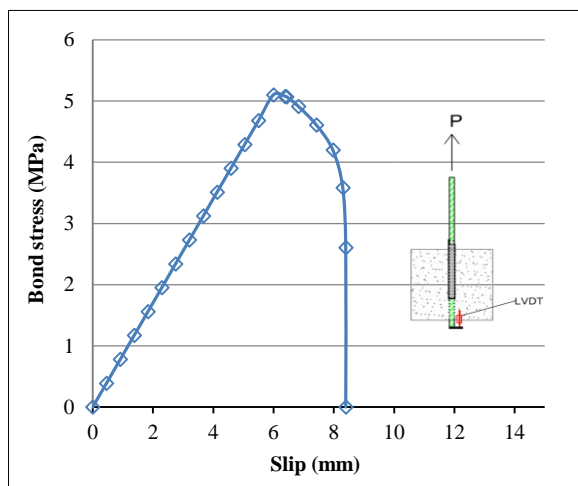
**Table 5. Pull-out test results**

| Name of specimens | Specimen | $\tau_{max}$ (MPa) | *Slip* (mm) | Strain ($10^{-6}$) | Failure pattern |
|---|---|---|---|---|---|
| GFRP-C (Centric) | 1 | 5.10 | 6.00 | 5291 | Pull out |
| | 2 | 5.17 | 7.70 | 4900 | |
| | 3 | 3.33 | 6.40 | 3728 | |
| | 4 | 4.64 | 4.53 | 5987 | |
| | 5 | 4.48 | 4.20 | 3934 | |
| | 6 | 4.25 | 2.74 | 5440 | |
| **Average** | | **4.49** | **5.26** | **4880** | |
| GFRP-E (Eccentric) | 1 | 1.65 | 4.31 | 1352 | Concrete crushed |
| | 2 | 1.87 | 2.94 | 2595 | |
| | 3 | 0.96 | 2.42 | 692 | |
| | 4 | 1.66 | 1.93 | 1467 | |
| | 5 | 1.96 | 4.17 | 2756 | |
| | 6 | 1.20 | 3.50 | 1862 | |
| **Average** | | **1.55** | **3.21** | **1787** | |

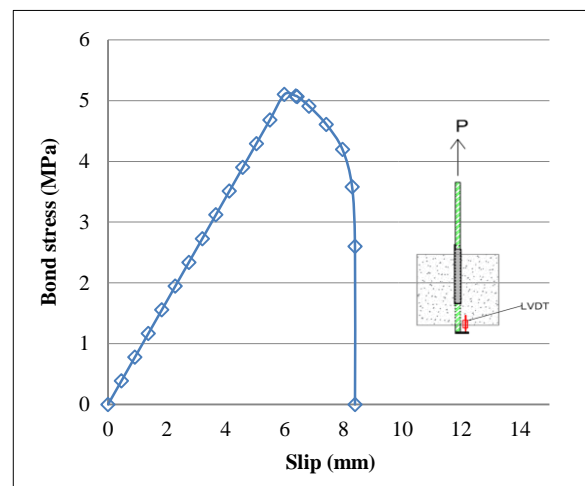| | | | | |
|---|---|---|---|---|
| | 1 | 1.58 | 3.47 | - |
| | 2 | 1.80 | 4.36 | 1979 |
| | 3 | 2.21 | 3.61 | 2525 |
| GFRP-C-Sheet (Eccentric + GFRP sheet) | 4 | 2.07 | 3.55 | 1754 | Debonding and concrete crushed |
| | 5 | 2.06 | 4.92 | 2976 |
| | 6 | 2.07 | 4.48 | 1314 |
| **Average** | | **1.96** | **4.07** | **1961** |

## 3.2. Bond Stress-Slip Relationship
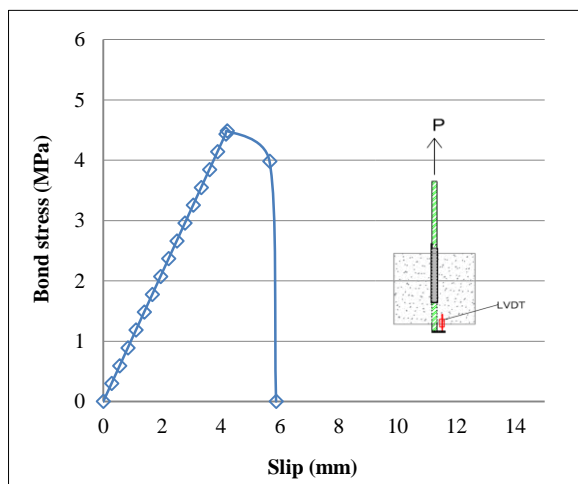
### 3.2.1. GFRP Bar Centric (GFRP-C)

Figure 7 shows the correlation between bond stress and slip value of the centric specimens (GFRP-C). As shown, the specimen had a low initial stiffness and a significant increase in displacement when the bond stress increased. This was because the bond stress in this test was primarily caused by adhesion and friction between the GFRP bars and the concrete, resulting in a low mechanical bearing due to the smooth surface of the GFRP bars. The bond stress and slip relationship behaved linearly until the maximum bond stress. Upon reaching the maximum stress, the load returns to zero without any significant slip. Then it can be assumed that after ultimate stress has been reached, the specimen no longer has the adhesive properties between GFRP bars and concrete. As shown in Table 5, the average maximum stress of GFRP-C was 4.49 MPa and the slip at the ultimate stress was 5.26 mm.
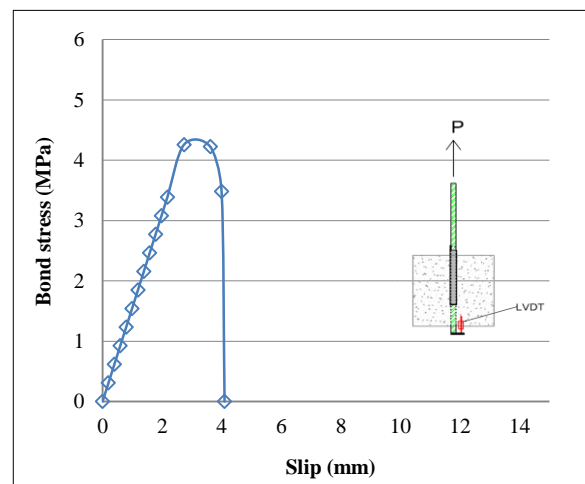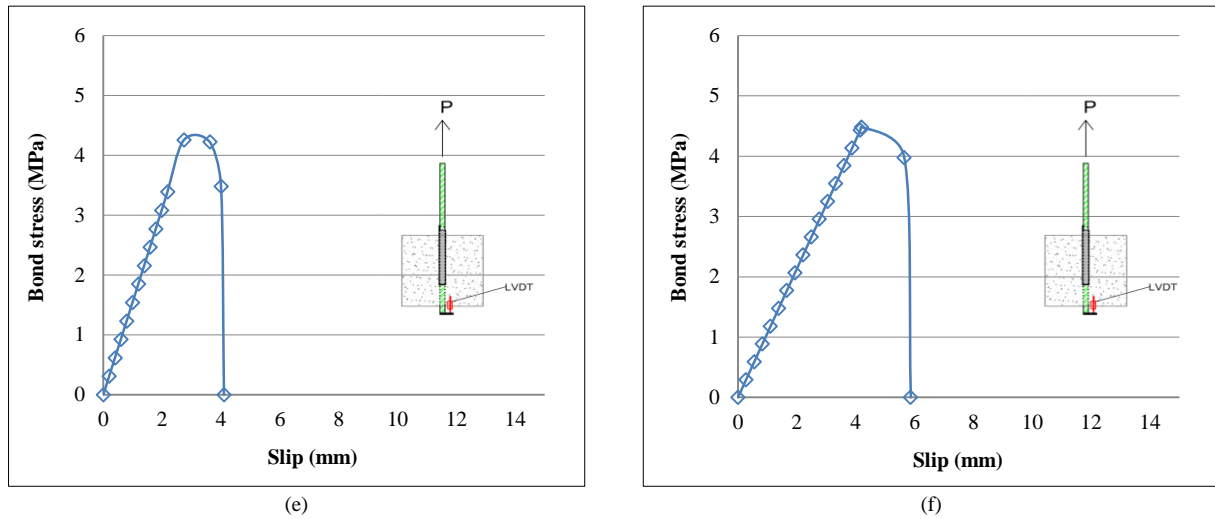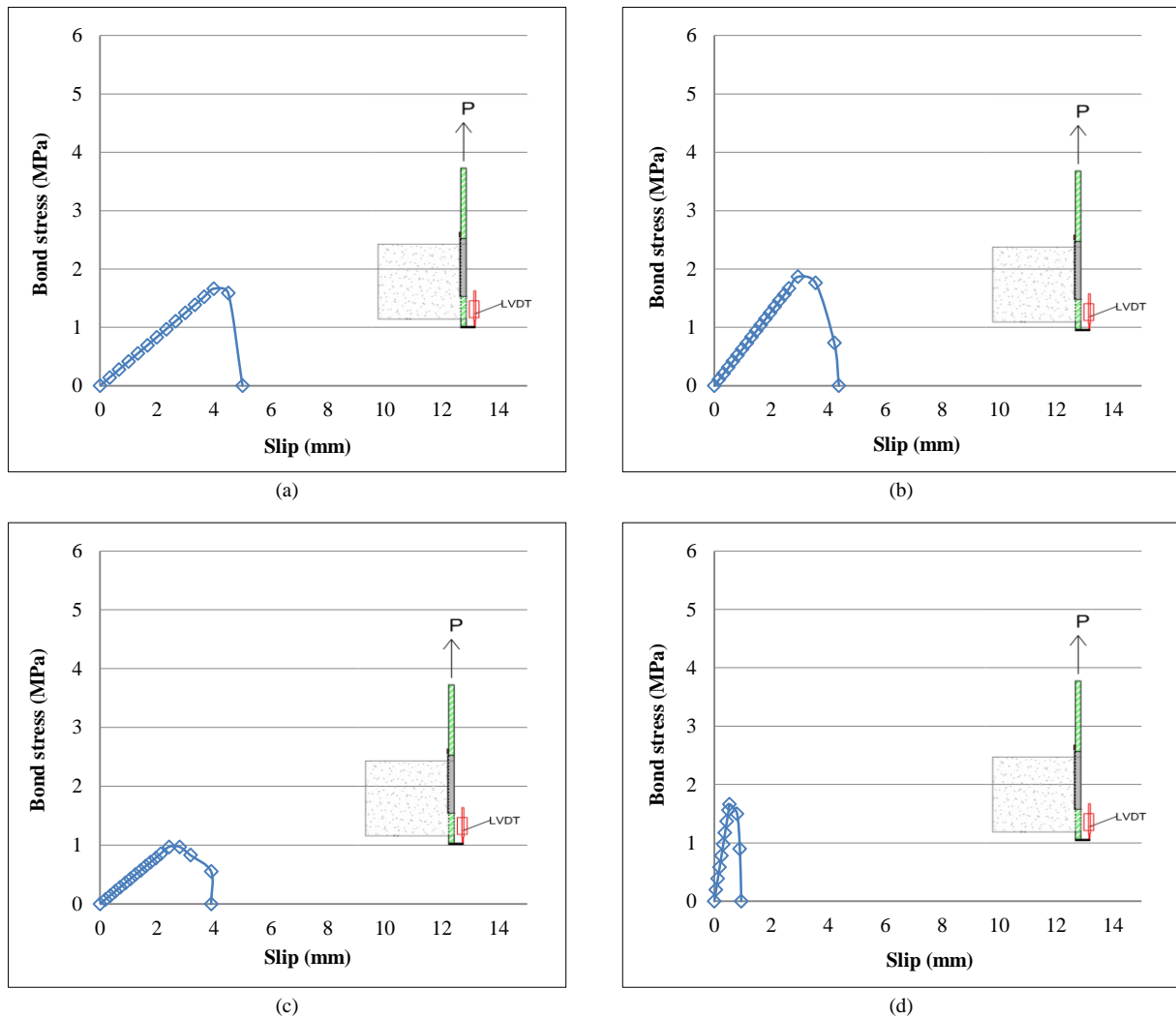


(a)



(b)



(c)



(d)

(e)                                                                                      (f)

**Figure 7. Bond stress-slip relationship of GFRP centric specimen**

The post-peak behavior of all centric specimens was ductile, where the bond stress gradually decreased after reaching its maximum stress. The same results were also reported in previous studies with centric pull-out tests [5, 15].

### 3.2.2. GFRP Bar Eccentric (GFRP-E)

This specimen was used to compare the effect of bar location on bond stress behavior. The position of the GFRP bar was at the edged (eccentric), thereby reducing the area of concrete-GFRP bar adhesion. Figure 8 shows the bond stress-slip relationships in eccentric specimens.
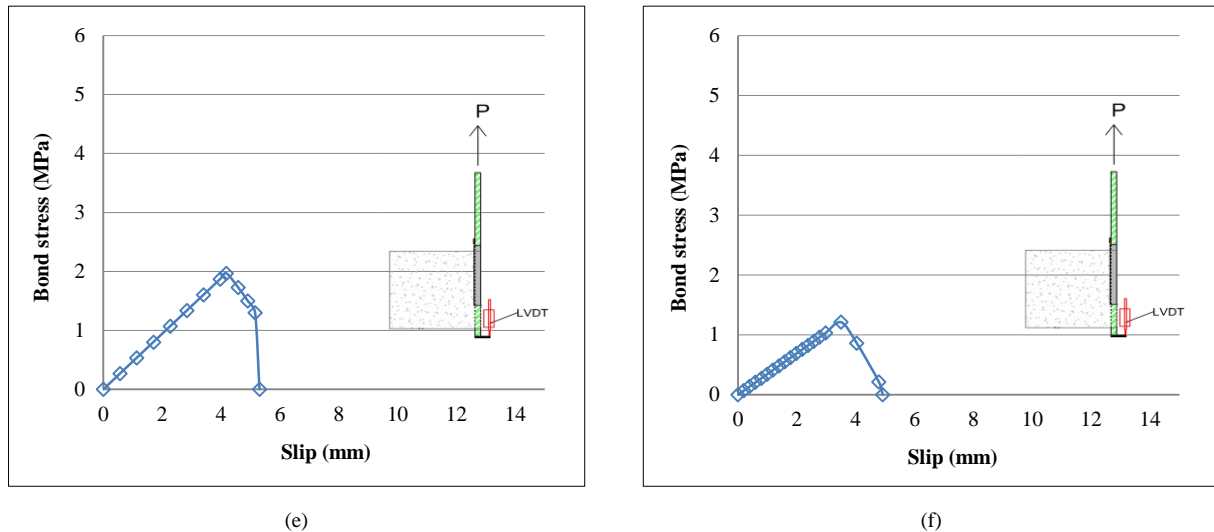


(a)                                                                                      (b)



(c)                                                                                      (d)

(e)　　　　　　　　　　　　　　　　　　　　　(f)

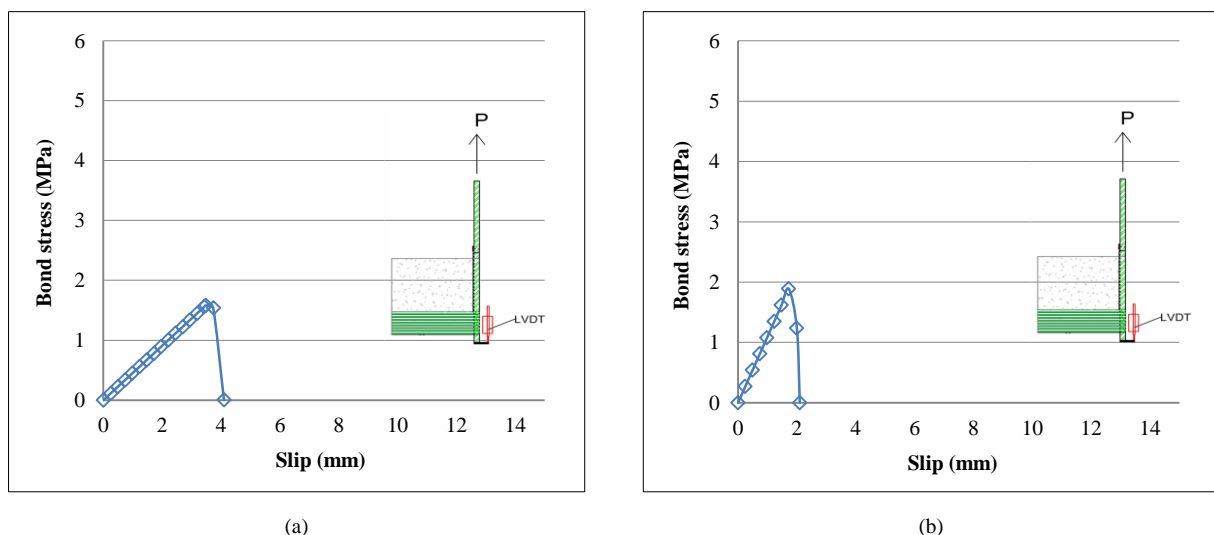**Figure 8. Bond stress-slip relationship of GFRP eccentric specimen (GFRP-E)**

The bond stress-slip behavior on the specimen showed a low initial stiffness. This was indicated by an increase in bond stress followed by a significant increase in slip. At the time of failure, bond stress averaged 1.55 MPa and the slip that occurred was 3.21 mm. The findings of the study revealed that the bond stress exhibited by the eccentric specimens was comparatively lower than that of the centric specimen. This was reasonable because the GFRP bar was positioned at the edge of the concrete. Hence the bond action from the adhesion and friction between rebar and concrete was reduced. The absence of a compressed zone around the bonded length is observed in the concrete. The level of confinement resulting from adhesion and friction between the rebar and concrete was reduced.

Eccentric pull-out specimens also showed smaller bond slip values than the centric specimens. This difference was about 63% compared to eccentric bars. Other researchers have shown similar where the lower slip values in eccentric tests [15, 28]. Veljkovic et al. [15] suggested that the slip values in eccentric specimens are subject to variation based on a range of factors, such as the strength of the concrete, the diameter of the bars, and the type of GFRP bars utilized.

### 3.2.3. GFRP Bar Eccentric with GFRP Sheet Confinement (GFRP-E-Sheet)

The addition of GFRP sheet to this specimen aims to increase the bonding strength of GFRP bars without concrete cover. Moreover, GFRP sheets are an external shear reinforcement in RC beam application. The bond stress-slip relationship is shown in Figure 9.

As can be seen, adding GFRP sheet confinement in eccentric bars significantly improved the initial stiffness compared to the eccentric specimens. This is because GFRP bars provide an additional confinement effect to GFRP bars, which enhances the bearing force of the bar and consequently leads to an increase in the bond strength to concrete. The average bond stress at failure was 1.96 MPa with a slip of 4.06 mm. These results were better than eccentric specimens without GFRP sheet.
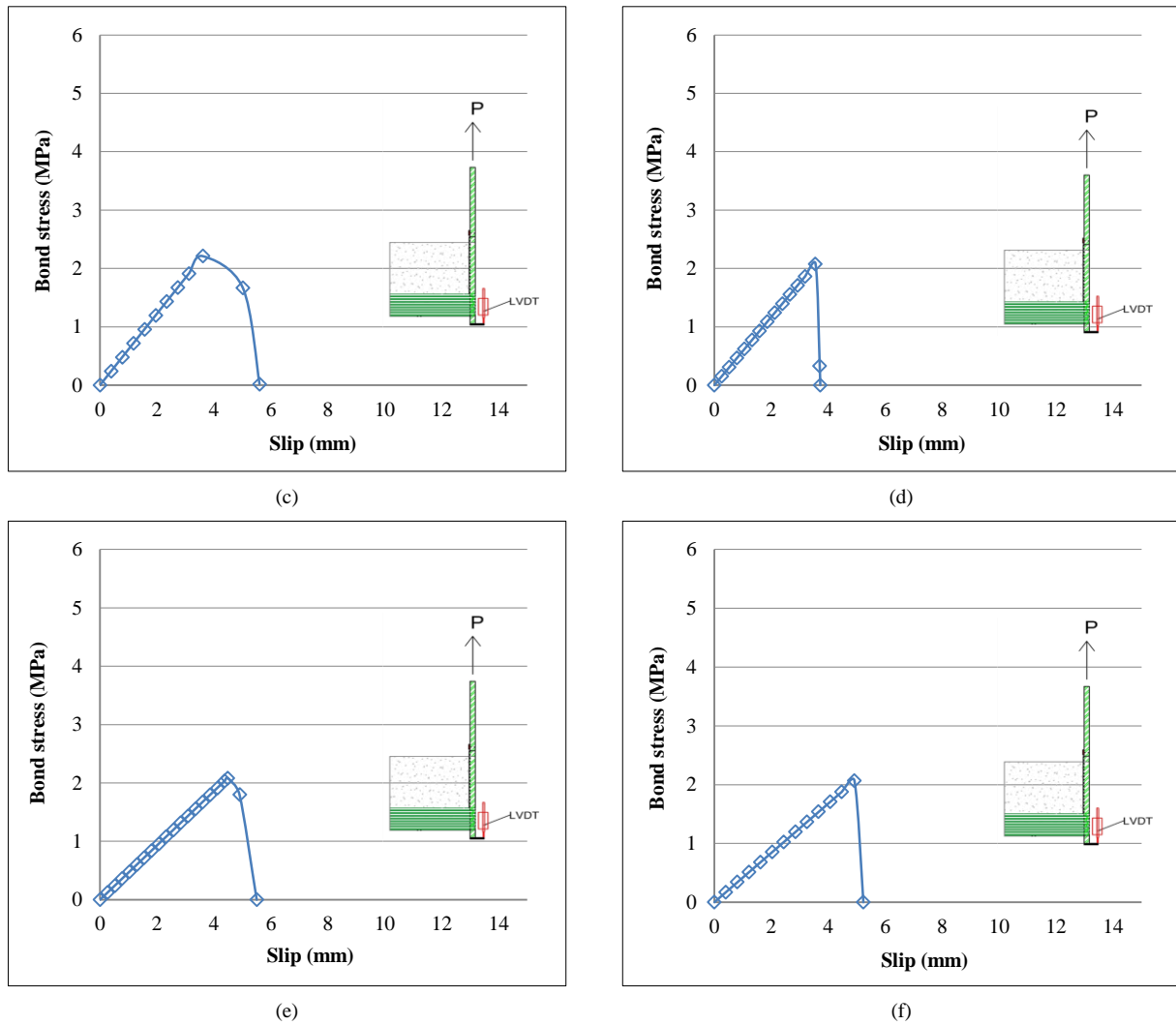


(a)　　　　　　　　　　　　　　　　　　　　　(b)

(c)



(d)



(e)



(f)

**Figure 9. Bond stress-slip relationship of GFRP eccentric + GFRP sheet (GFRP-E-Sheet)**

## 3.3. Comparison of Bond Stress-Slip Behavior

For each variation, one sample was selected and plotted in Figure 10. There were differences in the bond stress-slip behavior of the three specimens. The difference can be seen from the initial stiffness, maximum bond stress and maximum slip.
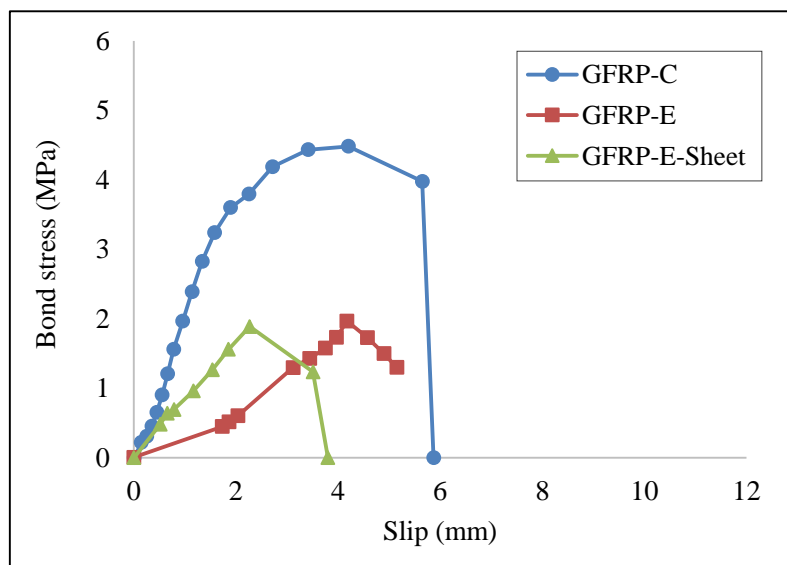


**Figure 10. Comparison of the third specimen bond stress-slip relationship**

Figure 10 shows that the change of reinforcement position from the middle to the edge significantly affected the initial stiffness of the test specimen. Specimens with centric rebar show the highest initial stiffness, while specimens with eccentric rebar show lower initial stiffness. Adding GFRP sheets to specimens with eccentric rebar can increase initial stiffness, but its increment has not been able to approach the initial stiffness of specimens with centric rebar.

Figure 10 also showed that the FRP bars position changed the failure pattern. Specimens with centric rebar exhibited more ductile behavior than eccentric rebar, which behaved more brittle. It was indicated from the bond-stress behavior where the load suddenly decreased due to the crushed concrete. The explanation regarding failure pattern will be explained in the next sub-chapter.

The use of GFRS sheet on GFRP-E-Sheet specimens provides confinement to concrete. This can delay the splitting crack and change the bond stress-slip behavior. As seen in Figure 10, the GFRP-E-Sheet specimens have higher initial stiffness and smaller slip values than the GFRP-E specimens.

### 3.4. Average Maximum Bond Stress

The average bond stress in each variation is shown in Figure 11. The effect of the position of the GFRP bars was discussed by comparing the average bond stress of GFRP-C and GFRP-E. Meanwhile, the effect of GFRP sheets was discussed from the test results of GFRP-E and GFRP-Sheet.
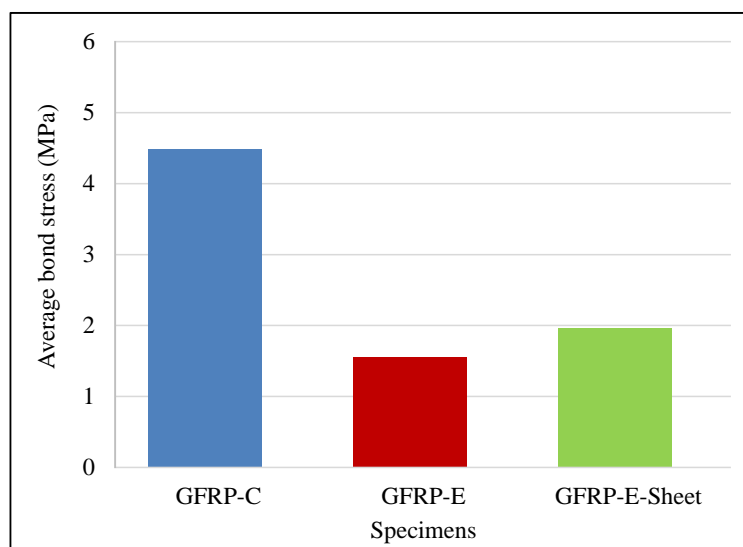


**Figure 11. Average maximum bonding stress**

According to Figure 11, the average maximum bonding stress of GFRP-E was reduced by 65% compared to that of GFRP-C. The study conducted by Aly et al. [29] also revealed that a decrease in concrete cover from four times to one time the bar diameter resulted in a 27% reduction in bond strength. The observed phenomenon can be attributed to the reduction in bonding area between the concrete and bars because GFRP bars were positioned at the edge of concrete. As the bond area is reduced, the bonding action resulting from the adhesion and friction between the reinforcement and the concrete will also be reduced. In addition, the addition of GFRP sheets to eccentric specimens was able to increase the average maximum bond stress by 26.4%. The observed increase can be attributed to the confinement stress generated by the GFRP sheet. Despite the increase in bond stress, the maximum bonding stress of GFRP-E-Sheet remained lower than that of the centric specimens.

The bond stress of FRP can be increased by creating the surface treatment of GFRP bars, such as sand-coated and various textures, as shown in Figure 12. The results of research conducted by Baena et al. [8] showed that surface treatment significantly affected bond stress.
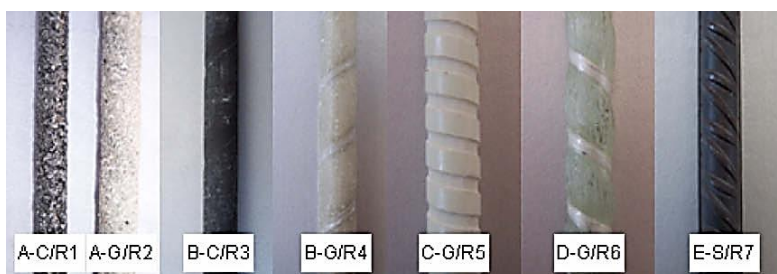


**Figure 12. Some surface treatment methods of FRP bars [8]**

### 3.5. Failure Pattern

Three types of failure patterns were observed: pull-out of GFRP bars (GFRP-C), concrete crushing (GFRP-E specimens), and debonding and concrete crushing (GFRP-C-Sheet). The failure patterns of the three variations of the test specimens are shown in Figure 13.
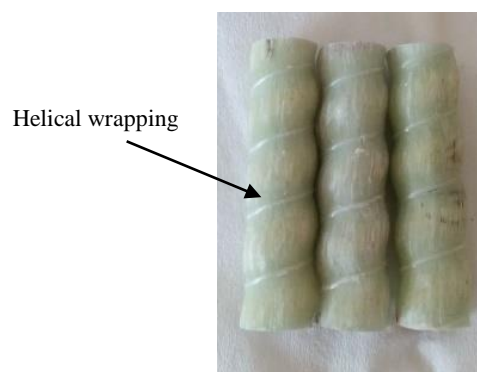


(a) GFRP-C specimens (centric)          (b) GFRP-E specimens (eccentric)



(c) GFRP-E-Sheet (eccentric + sheet)

**Figure 13. Failure Pattern**

### 3.5.1. GFRP Bar Centric (GFRP-C)

The centric specimen failed due to pull-out. This failure occurs for specimens with a sufficient concrete cover. The concrete cover can result in a confinement effect, also known as a bearing effect, on Glass Fiber Reinforced Polymer (GFRP) bars. The confinement effect can potentially decrease the possibility of crack formation in the concrete surrounding the bars. This can delay or even prevent splitting failure in centric specimens. Yan et al. [14] reported that more than 400 specimens failed by pull-out test, or around 60% of the data collected from previous studies. This failure occurs when the concrete cover-to-bar diameter (c/db) ratio is greater than or equal to 4.

The pull-out failure is due to a cut-off in the concrete between the ribs of the GFRP bars. The same phenomenon was observed in a study conducted by Wei et al. [28], which used the same type of bars in this study, namely the helical wrapping surface treatment, as shown in Figure 14.



Helical wrapping

**Figure 14. GFRP Bar with Helical Wrapping**

According to Wei et al. [28], the bonding stress on FRP bars with helical wrapping can be divided into axial shear forces and radial forces. The shear plane is produced from the ribs of GFRP bars and the concrete between the two ribs, as shown in Figure 15. Hence, the pull-out failure pattern is very dependent on the shear plane.
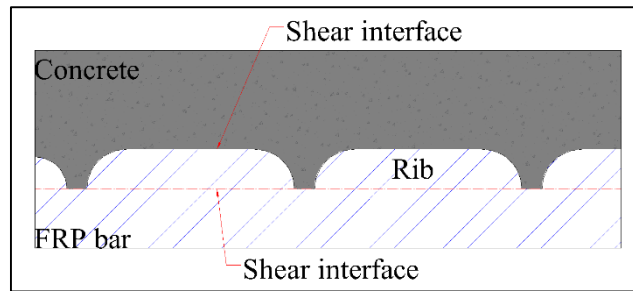
**Figure 15. Shear Interface between GFRP Bar Ribs and Concrete**

### 3.5.2. GFRP Bar Eccentric (GFRP-E)

Figure 13-b shows that all GFRP-E specimens failed due to the cracking of the concrete cover. Other researchers also reported that cracking of concrete cover and brittle post-peak behavior are features of eccentric tests [15, 23]. This phenomenon is because the confinement pressure produced by the concrete cover is insufficient, resulting in splitting failure before pull-out failure.

Wei et al. [28] suggested that the bonding mechanism between concrete and bars is attributed to chemical adhesion, friction, and mechanical interlocking. The present study did not account for chemical adhesion, and therefore, the mechanism of force transfer was attributed to friction and mechanical interlocking. Friction and mechanical interlocking can be divided by two components, namely axial and radial. The formation of tensile stress can be attributed to the radial component, as shown in Figure 16. In cases where the tensile stress exceeds the tensile strength of the concrete, the side of the concrete with the lowest resistance will experience cracking. In this particular case, the concrete located at the periphery is considered to be the most brittle component. Consequently, when subjected to the highest level of stress, the concrete in that region undergoes crushing, as shown in Figure 17.
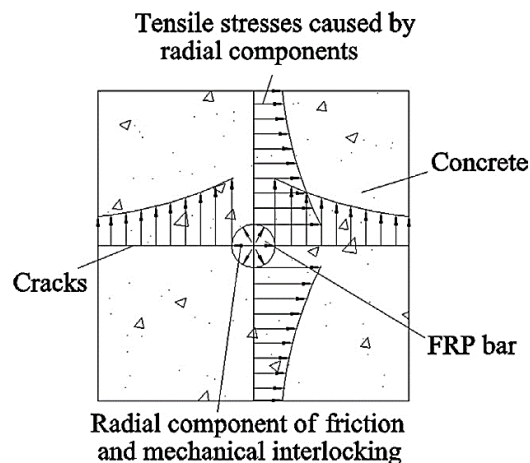


**Figure 16. Bonding action between FRP bars and concrete [28]**



**Figure 17. Concrete crushed on the weakest side of the concrete (edge side)**

### 3.5.3. GFRP Bar Eccentric + GFRP Sheet (GFRP-E-Sheet)

These specimens failed due to GFRP sheet debonding and concrete edge crushing. This bonding action results from friction, chemical adhesion, and mechanical interlocking. Chemical adhesion is produced by bonding the resin to the GFRP sheet. The resulting friction was also greater because of the additional friction from the bond between the GFRP bar and the GFRP sheet, as illustrated in Figure 18. Thus, the bond stress produced by this specimen was greater than that of the specimen without GFRP sheet (GFRP-E).
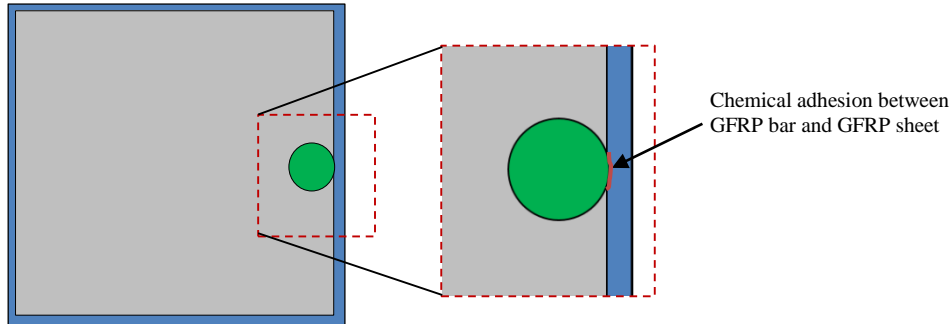


**Figure 18. Bonding between GFRP bar and GFRP sheet**

The failure pattern was initiated by debonding between the GFRP sheet and the concrete. Debonding was also known as a bond failure, characterized by separating the GFRP sheet from the concrete, as shown in Figure 19.



**Figure 19. Debonding between GFRP bar and GFRP sheet**

Following the debonding, a comparable mechanism was noted in the case of GFRP-E specimens, wherein the tensile stress in the concrete is caused by the radial force. The concrete undergoes crushing at its weakest points when the tensile stress exceeds its tensile strength.

## 4. Bond Strength Prediction using Design Codes

### 4.1. ACI 440.1R-06

As per the ACI 440.1R-06 [30], the bonding capacity between concrete and reinforcing bar can be calculated using Equation 3.

$$\frac{\tau_b}{0.083\sqrt{f'c}} = 4.0 + 0.3\frac{c}{d_b} + 100\frac{d_b}{l_d} \tag{3}$$

where $\tau_b$ is the bond strength (MPa), $d_b$ is the diameter of the bar, $l_d$ is the length of the bar embedded in concrete, $f'_c$ is the compressive strength of concrete (MPa) at 28 days, and $c$ is the minimum distance from the surface to the center of gravity of the bar or 1.5 times the center to the center distance of the bar.

### 4.2. Canadian Standards Association

The mean bond strength between bars and concrete specified by the CSA-S806-02 [31] is predicted using Equation 4.

$$\tau_b = \frac{d_{cs}\sqrt{f'c}}{1.15(K_1K_2K_3K_4K_5)\pi d_b}, \tag{4}$$

where $d_{cs}$ is the minimum distance between the concrete surface and the center of the bar, which is either taking 2/3 of the distance from the center to the center of the bar or directly measuring the minimum distance (mm). The value of $K_1$, representing the bar location factor, is 1.3 when horizontal bars are situated at a distance greater than 300 mm from the fresh concrete poured below the bar. In all other cases, the value of $K_1$ is 1.0. The factor $K_2$ is utilized to determine concrete density, with values of 1.3, 1.2, and 1.0 assigned, respectively to low-density, semi-low-density, and normal-density concrete. The value of the bar size factor denoted as $K_3$, is 0.8 when the bar area $A_b$ is less than or equal to 300 mm$^2$, and 1.0 when $A_b$ exceeds 300 mm$^2$. The value of the bar fiber factor denoted as $K_4$, is observed to be 1.0 for CFRP and GFRP, while it is 1.25 for Aramid Fiber Reinforced Polymer (AFRP). The $K_5$, which represents the surface profile factor of a bar, is determined based on the type of surface present. Specifically, if the surface is rough, sanded, or braided, the factor is assigned a value of 1.0. On the other hand, if the surface exhibits a spiral pattern or ribbed texture, the factor is assigned a value of 1.05. Finally, if the surface is intended for a specific purpose, the factor is assigned a value of 1.8.

## 4.3. JSCE

The bond strength between FRP bars and concrete, as outlined in the Japan Design Code (JSCE) [32], is primarily based on the adaptation of the equation for steel bars, as shown in Equation 5.

$$\tau_b = \frac{f_{bod}}{\alpha_1} \tag{5}$$

where $\alpha_1$ is a confinement modification factor defined as follows:

$$\alpha_1 = 1.0 \; for \; k_c \leq 1.0 \tag{5-a}$$

$$\alpha_1 = 0.9 \; for \; 1.0 < k_c \leq 1.5 \tag{5-b}$$

$$\alpha_1 = 0.8 \; for \; 1.5 < k_c \leq 2.0 \tag{5-c}$$

$$\alpha_1 = 0.7 \; for \; 2.0 < k_c \leq 2.5 \tag{5-d}$$

$$\alpha_1 = 0.6 \; for \; k_c > 2.5 \tag{5-e}$$

$$k_c = \frac{c}{d_b} + \frac{15A_t}{sd_b} \cdot \frac{E_t}{E_s} \tag{5-f}$$

$$f_{bod} = \frac{0.28\alpha_2 f_c^{2/3}}{1.3} \leq 3.2 \; N/mm^2 \tag{5-g}$$

where $c$ is the minimum value of the clear bottom distance from the tensile reinforcement or half of the clear distance between reinforcements. The equation also incorporates the cross-sectional area of transverse reinforcement, represented by $A_t$. The $s$ is the distance between the transverse reinforcement. $E_t$ and $E_s$ are the elastic modulus of the transverse reinforcement and steel, respectively. In addition, the equation involves the designed concrete bond strength, denoted as $f_{bod}$, and the modifying factor for the bond strength, represented by $\alpha_2$. It is important to note that the value of $\alpha_2$ is 1.0 when the bond strength is equal to or greater than the deformed steel bars. However, if the bond strength is less than the deformed steel bars, the value of $\alpha_2$ must be reduced according to the test results.

## 4.4. Comparison of Each Design Guideline

Table 6 compares the factors that have been considered, as well as the limitations in each design guideline, to calculate the bond strength between concrete and FRP bar.

**Table 6. Bond strength-affecting factors in design codes**

| Codes | Concrete strength | Bar diameter | Concrete cover | Bar location | Embedded length | Bar surface | Transverse confinement | Fiber type |
|---|---|---|---|---|---|---|---|---|
| ACI 440.1R-06 | ✓ | ✓ | ✓ | ✓ | ✓ | ✓ | x | x |
| CSA S806-02 | ✓ | ✓ | ✓ | ✓ | x | ✓ | x | ✓ |
| JSCE | ✓ | ✓ | ✓ | ✓ | x | x | ✓ | x |

Table 6 demonstrates that all codes have taken into account the variables of concrete strength, bar diameter, concrete cover, and location. The consideration of the embedded length factor is exclusively limited to ACI 440.1R-06. The inclusion of bar surface variation has been incorporated in CSA S806-02 and JSCE, whereas it has been neglected in ACI 440.1R-06. Meanwhile, the transverse reinforcement factor is only taken into account in JSCE. The fiber type used in reinforcement is only used in CSA S806-02.
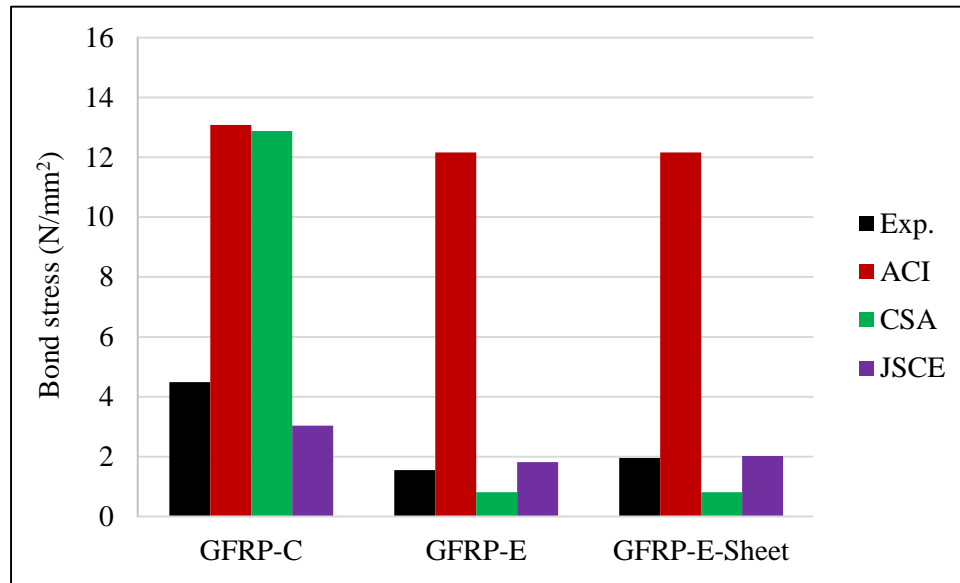
### 4.5. Comparison of Experiment and Calculation Results

The summary of the bond strength calculations for each design guideline is tabulated in Table 7 and the comparison with the experimental results is presented in Figure 20.

**Table 7. Bond strength comparison between experimental and calculation results**

| Specimens | Experiment | ACI | | CSA | | JSCE | |
|---|---|---|---|---|---|---|---|
| | $\tau_{EXP}$ (N/mm$^2$) | $\tau_{ACI}$ (N/mm$^2$) | $\tau_{EXP}/\tau_{ACI}$ | $\tau_{CSA}$ (N/mm$^2$) | $\tau_{EXP}/\tau_{CSA}$ | $\tau_{JSCE}$ (N/mm$^2$) | $\tau_{EXP}/\tau_{JSCE}$ |
| GFRP-C | 4.49 | 13.08 | 0.34 | 12.88 | 0.35 | 3.04 | 1.48 |
| GFRP-E | 1.55 | 12.16 | 0.13 | 0.82 | 1.90 | 1.82 | 0.85 |
| GFRP-E-Sheet | 1.96 | 12.16 | 0.16 | 0.82 | 2.40 | 2.02 | 0.97 |



**Figure 20. Comparison between experiments and predicted design codes**

On the centric specimens (GFRP-C), ACI and CSA codes overestimated the bond strength compared to the experimental results. The experimental comparison ratio with ACI and CSA calculation was 0.34 and 0.35, respectively (Table 7). These findings show that the difference ratio is significantly different and unsafe. On the other hand, the experimental findings revealed a higher bond strength than JSCE calculation, implying that the code was conservative. The ratio between the experimental and JSCE calculation results ($\tau_{EXP}/\tau_{JSCE}$) was 1.48.

On the eccentric specimens (GFRP-E), ACI code also overestimated the bond strength of the experimental result, with the $\tau_{EXP}/\tau_{ACI}$ was 0.13. The bond strength obtained from experimental results is smaller than those predicted using CSA, with the $\tau_{EXP}/\tau_{CSA}$ was 1.9. This result contrasts with the centric specimens, where the experimental results are significantly higher than the CSA calculations, with the $\tau_{EXP}/\tau_{CSA}$ was 0.35. This is because the effect of the embedded length has not been considered in CSA. As a result, specimens without embedding length have greater accuracy than specimens with embedding length. This study assumes that the eccentric specimens do not have an embedment length or the effect is minimal. In addition, only JSCE predicts the bond strength of eccentric bars close to the measured values in the experimental investigation. The ratio between the experiment and calculation using JSCE code ($\tau_{EXP}/\tau_{JSCE}$) was 0.85.

The eccentric bars, with the addition of the GFRP sheet, also showed almost the same results as the centric specimens. The outcomes of computations using ACI exhibit a significant difference when compared to the findings of the experiments. While the results of the calculation using CSA are smaller than the experimental results. It should be noted that the ACI and CSA have not considered the transverse reinforcement factor, whereas, in this study, the transversal reinforcement is the GFRP sheet. Thus, the results of eccentric calculations with and without GFRP sheets showed the same results. Instead, JSCE showed the highest level of accuracy compared to other codes and the results were very close to the results of the experiment ($\tau_{EXP}/\tau_{JSCE} = 0.97$). This is because JSCE has considered the influence of transverse reinforcement that corresponds to the design of the eccentric specimens with the additional GFRP sheet.

## 5. Conclusions

Based on the results of the pull-out test on three variations of specimens, which were centric specimens (GFRP-C), eccentric specimens (GFRP-E), and eccentric in combination with GFRP bars (GFRP-E-Sheet), the following conclusions can be drawn:

- The bond behavior between fiber-reinforced polymer (FRP) bars and concrete is dependent on the location of the bars and the presence of transverse reinforcement (GFRP sheet in this study). The change in the location of FRP bars from a centric to an eccentric position result in a reduction in bond strength and stiffness, as well as changes in the failure mode. The combination of eccentric bars and FRP sheets as transverse reinforcement results in an enhancement of both bond strength and stiffness.

- The centric bars demonstrated ductile bonding behavior and failed due to pull-out. The eccentric bars demonstrated brittle bond characteristics, resulting in a sudden drop in load due to concrete crushing. The eccentric bars, when used in combination with the GFRP sheet, exhibited brittle failure caused by debonding between the GFRP sheet and concrete, followed by crushing of the concrete at the specimen edges.

- The evaluation of bond strength through a comparative analysis of experimental and calculated results utilizing design guidelines reveals a varying degree of accuracy due to several unaccounted factors in the guidelines. The ACI and CSA codes exhibit significantly greater values in comparison to the experimental results obtained from the centric specimens. In contrast, JSCE standards indicate relatively lower results. Among the various codes, JSCE exhibited the highest degree of accuracy, while ACI resulted in overestimated results for the eccentric specimens.

## 6. Declarations

### 6.1. Author Contributions

Conceptualization, R.D.; methodology, F. and K.; formal analysis, F., K., and R.I.; investigation, F. and K.; writing—original draft preparation, F.; writing—review and editing, R.D., R.I., S.H., and L.N.N.; visualization, K.; supervision, R.D. All authors have read and agreed to the published version of the manuscript.

### 6.2. Data Availability Statement

The data presented in this study are available on request from the corresponding author.

### 6.3. Funding

### 6.4. Acknowledgements

### 6.5. Conflicts of Interest

The authors declare no conflict of interest.

## 7. References

[1] Balafas, I., & Burgoyne, C. J. (2010). Environmental effects on cover cracking due to corrosion. Cement and Concrete Research, 40(9), 1429–1440. doi:10.1016/j.cemconres.2010.05.003.

[2] Djamaluddin, R., Hijriah, Irmawati, R., Faharuddin, & Wahyuningsih, R. T. (2019). Delamination mechanism of GFRP sheet bonded on the reinforced concrete beams. MATEC Web of Conferences, 258, 03009. doi:10.1051/matecconf/201925803009.

[3] Solyom, S., & Balázs, G. L. (2020). Bond of FRP bars with different surface characteristics. Construction and Building Materials, 264, 11983. doi:10.1016/j.conbuildmat.2020.119839.

[4] Nanni, A., De Luca, A., & Jawaheri Zadeh, H. (2014). Reinforced Concrete with FRP Bars. In Reinforced Concrete with FRP Bars. CRC Press, London, United Kingdom. doi:10.1201/b16669.

[5] Solyom, S., Di Benedetti, M., Szijártó, A., & L. Balázs, G. (2018). Non-Metallic Reinforcements with Different Moduli of Elasticity and Surfaces for Concrete Structures. Architecture, Civil Engineering, Environment, 11(2), 79–88. doi:10.21307/acee-2018-025.

[6] Brown, V. L., & Bartholomew, C. L. (1993). FRP reinforcing bars in reinforced concrete members. ACI Materials Journal, 90(1), 34–39. doi:10.14359/4034.

[7] Pecce, M., Manfredi, G., Realfonzo, R., & Cosenza, E. (2001). Experimental and Analytical Evaluation of Bond Properties of GFRP Bars. Journal of Materials in Civil Engineering, 13(4), 282–290. doi:10.1061/(asce)0899-1561(2001)13:4(282).

[8] Baena, M., Torres, L., Turon, A., & Barris, C. (2009). Experimental study of bond behaviour between concrete and FRP bars using a pull-out test. Composites Part B: Engineering, 40(8), 784–797. doi:10.1016/j.compositesb.2009.07.003.

[9] Achillides, Z., & Pilakoutas, K. (2004). Bond Behavior of Fiber Reinforced Polymer Bars under Direct Pullout Conditions. Journal of Composites for Construction, 8(2), 173–181. doi:10.1061/(asce)1090-0268(2004)8:2(173).

[10] Yan, F., & Lin, Z. (2016). New strategy for anchorage reliability assessment of GFRP bars to concrete using hybrid artificial neural network with genetic algorithm. Composites Part B: Engineering, 92, 420–433. doi:10.1016/j.compositesb.2016.02.008.

[11] Belarbi, A., & Wang, H. (2012). Bond Durability of FRP Bars Embedded in Fiber-Reinforced Concrete. Journal of Composites for Construction, 16(4), 371–380. doi:10.1061/(asce)cc.1943-5614.0000270.

[12] Abbasi, A., & Hogg, P. J. (2005). Temperature and environmental effects on glass fibre rebar: Modulus, strength and interfacial bond strength with concrete. Composites Part B: Engineering, 36(5), 394–404. doi:10.1016/j.compositesb.2005.01.006.

[13] Lin, X., & Zhang, Y. X. (2014). Evaluation of bond stress-slip models for FRP reinforcing bars in concrete. Composite Structures, 107(1), 131–141. doi:10.1016/j.compstruct.2013.07.037.

[14] Yan, F., Lin, Z., & Yang, M. (2016). Bond mechanism and bond strength of GFRP bars to concrete: A review. Composites Part B: Engineering, 98, 56–69. doi:10.1016/j.compositesb.2016.04.068.

[15] Veljkovic, A., Carvelli, V., Haffke, M. M., & Pahn, M. (2017). Concrete cover effect on the bond of GFRP bar and concrete under static loading. Composites Part B: Engineering, 124, 40–53. doi:10.1016/j.compositesb.2017.05.054.

[16] Jurić, A., & Štefić, T. (2022). Experimental Comparison of the Bearing Capacity of GFRP Beams and 50% Recycled GFRP Beams. Civil Engineering Journal, 8(12), 3902-3911. doi:10.28991/CEJ-2022-08-12-017.

[17] Liang, K., Chen, L., Shan, Z., & Su, R. K. L. (2023). Experimental and theoretical study on bond behavior of helically wound FRP bars with different rib geometry embedded in ultra-high-performance concrete. Engineering Structures, 281, 115769. doi:10.1016/j.engstruct.2023.115769.

[18] Shan, Z., Liang, K., & Chen, L. (2023). Bond behavior of helically wound FRP bars with different surface characteristics in fiber-reinforced concrete. Journal of Building Engineering, 65, 105504. doi:10.1016/j.jobe.2022.105504.

[19] Chen, L., Liang, K., & Shan, Z. (2023). Experimental and theoretical studies on bond behavior between concrete and FRP bars with different surface conditions. Composite Structures, 309, 116721. doi:10.1016/j.compstruct.2023.116721.

[20] Li, P., Zeng, J., Li, W., & Zhao, Y. (2022). Effect of concrete heterogeneity on interfacial bond behavior of externally bonded FRP-to-concrete joints. Construction and Building Materials, 359, 129483. doi:10.1016/j.conbuildmat.2022.129483.

[21] Nepomuceno, E., Sena-Cruz, J., Correia, L., & D'Antino, T. (2021). Review on the bond behavior and durability of FRP bars to concrete. Construction and Building Materials, 287, 123042. doi:10.1016/j.conbuildmat.2021.123042.

[22] Fahmy, M. F. M., ShehabEldeen, A. S. A., & Wu, Z. (2021). Bar surface treatment effect on the bond-slip behavior and mechanism of basalt FRP bars embedded in concrete. Construction and Building Materials, 289, 122844. doi:10.1016/j.conbuildmat.2021.122844.

[23] Galati, N., Nanni, A., Dharani, L. R., Focacci, F., & Aiello, M. A. (2006). Thermal effects on bond between FRP rebars and concrete. Composites Part A: Applied Science and Manufacturing, 37(8), 1223–1230. doi:10.1016/j.compositesa.2005.05.043.

[24] Alsayed, S., Al-Salloum, Y., Almusallam, T., El-Gamal, S., & Aqel, M. (2012). Performance of glass fiber reinforced polymer bars under elevated temperatures. Composites Part B: Engineering, 43(5), 2265–2271. doi:10.1016/j.compositesb.2012.01.034.

[25] Wang, Y. C., Wong, P. M. H., & Kodur, V. (2007). An experimental study of the mechanical properties of fibre reinforced polymer (FRP) and steel reinforcing bars at elevated temperatures. Composite Structures, 80(1), 131–140. doi:10.1016/j.compstruct.2006.04.069.

[26] Dong, K., Hao, J., Li, P., & Zhong, C. (2022). A nonlinear analytical model for predicting bond behavior of FRP-to-concrete/steel substrate joints subjected to temperature variations. Construction and Building Materials, 320, 126225. doi:10.1016/j.conbuildmat.2021.126225.

[27] ACI440.3R. (2004). Guide Test Methods for Fiber-Reinforced Polymers (FRPs) for Reinforcing or Strengthening Concrete Structures. American Concrete Institute (ACI), Farmington Hills, United States.

[28] Wei, W., Liu, F., Xiong, Z., Lu, Z., & Li, L. (2019). Bond performance between fibre-reinforced polymer bars and concrete under pull-out tests. Construction and Building Materials, 227, 116803. doi:10.1016/j.conbuildmat.2019.116803.

[29] Aly, R. (2007). Stress along tensile lap-spliced fibre reinforced polymer reinforcing bars in concrete. Canadian Journal of Civil Engineering, 34(9), 1149–1158. doi:10.1139/L07-046.

[30] ACI 440.1R-06. (2006). Guide for the design and construction of structural concrete reinforced with FRP bars. American Concrete Institute (ACI), Farmington Hills, United States.

[31] CSA-S806-02. (2002). Design and construction of building components with fibre reinforced polymers. Canadian Standards Association (CSA), Toronto, Canada.

[32] Uomoto, T. (1997). Recommendation for design and construction of concrete structures using continuous fiber reinforcing materials. Japan Society of Civil Engineers, Tokyo, Japan.